Biosensors and Bioelectronics 25 (2010) 1363–1369

Contents lists available at ScienceDirect

Biosensors and Bioelectronics

journal homepage: www.elsevier.com/locate/bios

Hydrodynamic focusing of conducting fluids for conductivity-based biosensors

Mansoor Nasir, Daniel A. Ateya, Diana Burk, Joel P. Golden, Frances S. Ligler*

Naval Research Lab, Center for Bio/Molecular Science and Engineering, 4555 Overlook Ave SW., Washington, DC 20375, USA

ARTICLE INFO

Article history:
Received 19 August 2009
Received in revised form 20 October 2009
Accepted 21 October 2009
Available online 30 October 2009

Keywords:
Conductivity
Flow-focusing
Biosensor
Reynolds number
Magnetic beads
Hydrodynamic focusing

ABSTRACT

Hydrodynamic focusing of a conducting fluid by a non-conducting fluid to form a constricted current path between two sensing electrodes is implemented in order to enhance the sensitivity of a 4-electrode conductance-based biosensor. The sensor has a simple two-inlet T-junction design and performs four-point conductivity measurements to detect particles immobilized between the sensing electrode pair. Computational simulations conducted in conjunction with experimental flow studies using confocal microscopy show that a flat profile for the focused layer is dependent on the Reynolds number for the chosen flow parameters. The results also indicate that a flat focused layer is desirable for both increased sensitivity as well as surface-binding efficiency. Proof of concept for conductance measurements in a hydrodynamically focused conducting fluid was demonstrated with entrapped magnetic beads.

Published by Elsevier B.V.

1. Introduction

Historical uses of impedance measurements for acquiring biological information include: counting and sizing of suspended cells, assessing metabolic activity of bacteria, and monitoring cell proliferation and morphology in culture. The ability to fabricate electrodes in surfaces as well as in micron-scale chambers and microfluidic channels has enabled the enhancement of sensitivity and resolution compared with macroscale techniques. Impedance measurements in microchambers with antibody-coated electrodes have been used to detect *Escherichia coli* at concentrations as low as 10^5 colony forming units (cfu)/mL (Radke and Alocilja, 2005). However, the sensitivity is limited by the trade-off between the dimensions of the microchamber containing the cells suspended in conducting fluid and the need to prevent clogging.

Parallel laminar flow of liquids in microchannels has been studied extensively over the past decade for use in chemical and biological patterning of flows and surfaces, diffusional T-sensors, flow cytometry on a chip, and a variety of other microfluidic sensor applications (Atencia and Beebe, 2005; Brody et al., 1996; Hatch et al., 2001; Huh et al., 2005; Simonnet and Groisman, 2006; Ismagilov et al., 2000; Lee et al., 2006; Walsh et al., 2007). Of particular interest to the sensor community is the development of methods to direct target analytes to a sensor surface (Golden et al., 2007; Munson et al., 2004). Using a focusing stream to confine the sample stream to a narrow layer at the sensing surface was first described by Manz (Hofmann et al., 2002) as a way to use relatively large channels that are minimally susceptible to clogging. Papers employing such an approach generally assume that the focused layer is planar or flat (Munson et al., 2004; Stiles et al., 2005; Walsh et al., 2007; Huh et al., 2007). Indeed, any curvature in the sample stream profile is not apparent in micrographs taken from the side or top of the channel. However, in this paper, we document that the sample stream flowing along the sensor surface may not be flat but rather can be curved. This curving is prominent along the walls of the channel and depends on the *Re* and the geometry of the system. In the case of microarrays, this would lead to uneven exposure of the array to the target analytes in the sample. In the case of sensors based on evanescent illumination (total internal reflectance, surface plasmon resonance, and interferometry), a high proportion of the target analytes might pass through the channel without being exposed to the surface-bound recognition molecules being interrogated. Hydrodynamic focusing of a conductive layer has also been used to make an impedance-based microfluidic Coulter counter (Larsen et al., 1997; Rodriguez-Trujillo et al., 2008; Simonnet and Groisman, 2006; Hua and Pennell, 2009). In this case as well, the shape of the focused layer can have a major impact on the change in resistance between surface electrodes. In a sample stream with a curved profile, the change in resistance would be a function of the location of the cell in the sample stream. For evenly distributed placement of the target analytes at the surface, for interrogation optically or electronically, the sample stream needs to be as flat as possible.

* Corresponding author. Tel.: +1 202 404 6002; fax: +1 202 767 9594.
E-mail address: frances.ligler@nrl.navy.mil (F.S. Ligler).

0956-5663/$ – see front matter. Published by Elsevier B.V.
doi:10.1016/j.bios.2009.10.033

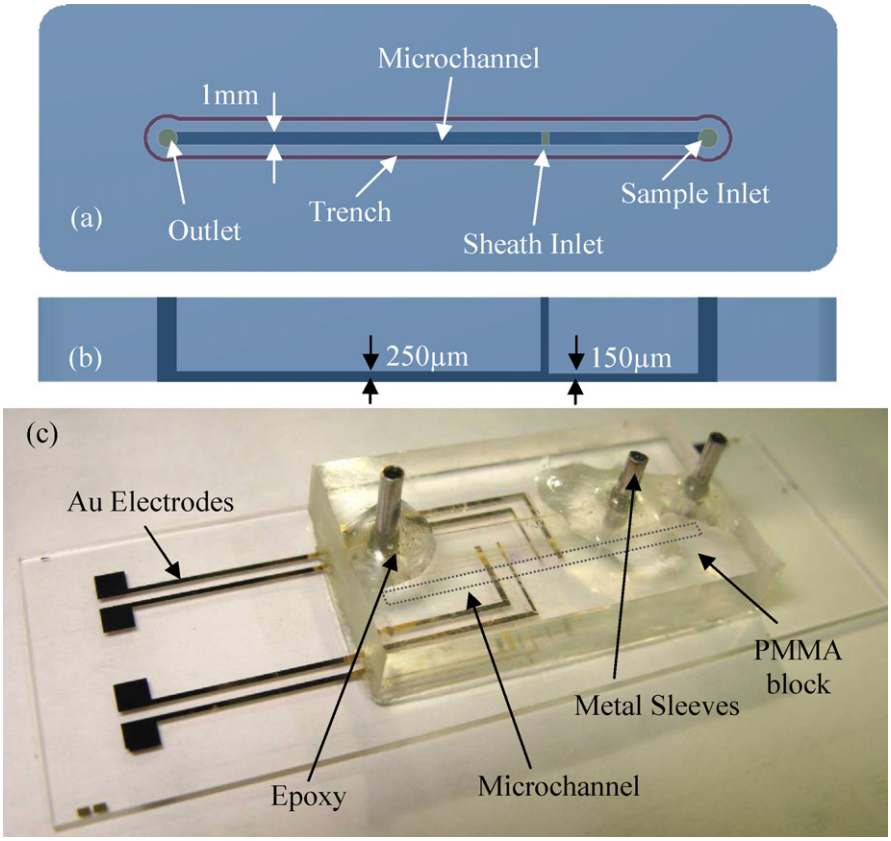

Fig. 1. (a) Top view of the device shows the sheath and sample inlets and the outlet. The sheath inlet is 250 μm × 1 mm. A 500 μm wide trench traces the boundaries of the channel. (b) Side view of the device shows the step change in height between the two sections of the microchannel. (c) The bottom figure shows an assembled device with the metal tubes for the inlets and outlet port. The device is machined out of a 6.5 mm thick PMMA block. The Au electrodes were patterned on standard glass slides and then attached to the PMMA piece using UV glue.

In this paper, we describe hydrodynamic focusing of a conducting fluid (phosphate buffer saline or PBS) by a non-conducting fluid (deionized H_2O) over a surface including the electrodes and captured cells or particles. A four-electrode system is implemented wherein the resistance between the two inner electrodes can be measured as a constant current is passed between the two outer electrodes (Hua and Pennell, 2009). In the process of characterizing the hydrodynamically focused conducting stream, we identified factors that affect the shape of that layer. First, we demonstrate that the curvature is in fact shaped primarily by the imprint of the velocity profile of the faster flowing sheath fluid. The flow rates are sufficiently high that diffusive mass transport is negligible. The results from numerical and experimental studies are used together to identify the relevant parameters that can be manipulated to control the shape of the stream profile.

In addition to numerical models and confocal microscopy, resistance measurements through the focused layer document differential conducting properties of fluid layers of varying depth. Using the optimally focused streams, decreasing the height of the focused conducting stream resulted in increased sensitivity of the conductivity-based sensor.

2. Experimental

2.1. Microchannel fabrication and assembly

The T-junction microchannel design used in this study confined the flow from the sample inlet to the bottom of the channel using a single sheath stream. The rectangular flow channel had the sheath stream inlet at 90° with respect to the sample stream inlet and the outlet as shown in Fig. 1(a). A T-junction design with rectangular channels facilitates rapid prototyping using standard micromachining and fabrication techniques. In addition, since only a single sheath stream is used, the microfluidic control is simple and easily miniaturized. Rectangular channels were easily milled and compatible with attachment to the glass microelectrode substrate.

The devices were milled from polymethyl methacrylate (PMMA) (Plexiglas G, Atofina Chemical, Inc., Philadelphia, PA) using a HAAS Mini Mill (HAAS Automation, Inc., Oxnard, CA). The channel and sheath inlet were machined using a 0.01 in. long-reach endmill. A 0.031 in. endmill was used for the sample inlet and outlet (Harvey Tool, Rowley, MA). Micromachining allows for rapid prototyping and high throughput. A trench 500 μm wide and 200 μm deep was milled at a distance of 500 μm from the outer edges of the microchannel and the inlets. This trench prevented the glue from leaking into the microchannel (Leatzow et al., 2002). A drill press was used to widen the upper half of the inlets and outlet where 0.023 in. wide metal tubing was inserted and glued into place using 5-min epoxy (Devcon, Danvers, MA). All the channels used in this particular study were 1 mm wide. The length of the channel from the first inlet to the outlet was 3 cm. The height of the channel for the section between the two inlets was approximately 150 μm and increased to 250 μm after the second inlet (Fig. 1(b)). This step design facilitated creation of a flatter focused stream and also reduced the convective mixing by lowering the point where the sample and sheath streams first come into contact with each other.

Microelectrodes were patterned on borosilicate glass slides using standard photolithography techniques. Slides were first piranha cleaned for 20 min. The electrodes were patterned using a 1 μm thick layer of negative photoresist (NR7 1000PY-Futurex).

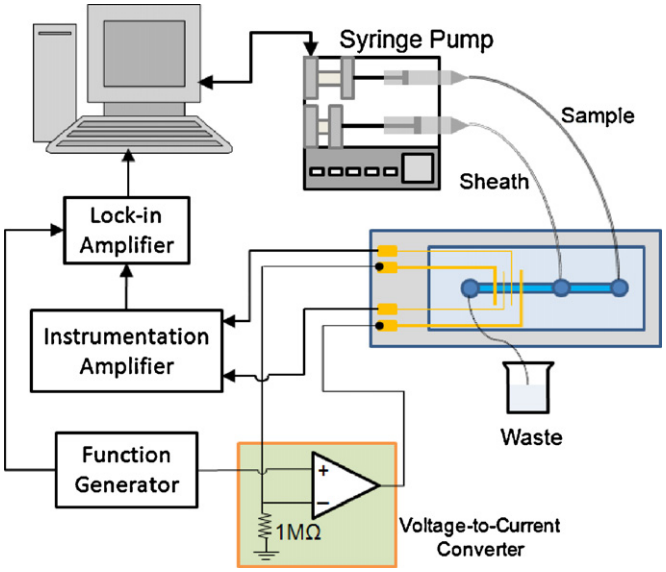

Fig. 2. In a voltage-to-current converter circuit the operational amplifier tries to keep the voltage at the two terminals equal. The current through the circuit is determined by the choice of the input voltage and the resistance of the grounded resistor on the negative terminal of the op-amp (1 V signal implies a current of 1 μA with a 1 MΩ resistor). Since the op-amp itself draws negligible current, the current flows from the op-amp output, through the outer electrodes and then to ground. Regardless of the resistance between the electrodes, the op-amp adjusts the output potential to supply a constant current.

An electron beam evaporator was used to deposit a film of gold (3000 nm) onto the slides with a thin film of titanium (300 Å) as the adhesion layer. Afterwards, the electrodes were defined by photoresist lift-off in acetone. The thickness of the electrodes is insignificant when compared to the focused stream and does not affect the flow-focusing. The two sense electrodes are 250 μm wide and 2 mm apart. The working electrodes are 500 μm wide and the separation between sense and working is 1 mm. The working electrodes are designed to be wider to reduce electrode polarization due to surface charge density and prevention of corrosion. The PMMA pieces were glued to standard microscope slides with electrodes using UV-curable adhesive (Optical Adhesive #72, Norland Products, Cranbury, NJ). A fully assembled channel is shown in Fig. 1(c).

2.2. Confocal studies

To visualize the three-dimensional concentration profile in microchannels during flow focusing studies, we used a Nikon Eclipse TE2000-E inverted microscope equipped with a Nikon D-Eclipse C1si confocal spectral imaging system (Nikon, Japan). As depicted in Fig. 2(a), confocal images were obtained by scanning in the region immediately downstream from where the sheath and sample streams intersect. Hydrodynamic focusing experiments were performed using deionized water for the sheath flow from the vertical inlet and deionized water mixed with FWT Red Powder fluorescent dye (Bright Dyes, Miamisburg, OH) for visualization of the flow from sample stream inlet.

A dual-syringe pump (Harvard Apparatus Model 33) provided precise control of the flow rates and flow-rate ratios. Confocal microscopy was performed using a 10× objective (NA 0.45, WD 4.00 Dry). Image resolution was 512 × 512 pixels with a Z-step size spacing of 5 μm and a pixel dwell time of 7.06 μs. A 40 mW argon laser was used at the 514.5 nm excitation line, and the spectral detector of the confocal imaging system was set to detect emission between 583 and 593 nm. The sheath and sample flow rates were chosen such that the flow-rate ratios were between 10 and 30. Image stacks were rendered and analyzed in three-dimensions using NIS-Elements AR confocal image processing software (Nikon, Japan). The three-dimensional concentration profile of the fluid flow in the channel was studied under various flow focusing conditions, varying both flow rates and flow-rate ratios.

2.3. Experimental setup

For conductivity measurements, a four-electrode measurement scheme was used. Four-electrode conductivity measurement systems are more robust than their two-electrode counterparts as the sensing electrodes are isolated from the current-carrying electrodes, thus reducing the undesirable polarization effects on the measurement of interest (Schwan, 1968). A voltage-to-current converter circuit was pulsed by a 240 Hz square-wave voltage input from a function generator (Tektronix AWG 5102), resulting in a 0.5 μA peak-to-peak current at the outer two (working) electrodes (Fig. 2). The voltage from the inner two (sense) electrodes was filtered and amplified with a high input impedance instrumentation amplifier (Warner Instruments DP-311). A lock-in amplifier (Stanford Research Systems SR10) was used to account for the phase shift between the measured signal from the instrumentation amplifier and the source signal from the function generator. The output signal of the lock-in amplifier was electronically recorded using a data acquisition card (National Instruments 6251) and a LabVIEW interface (National Instruments). The same software interface was also used to program a dual-syringe pump (Harvard Apparatus Model 33) for sheath and sample flow rates.

2.4. Numerical simulations

In addition to confocal microscopy, finite element modelling of the channels was performed using the COMSOL Multiphysics finite element analysis package (COMSOL Inc., Palo Alto, CA). In these simulations, the effects of changing sheath and sample flow rates, the flow-rate ratio and the presence of particles were considered. The simulations were conducted in three steps. First, solving the Navier–Stokes momentum equation:

$$\nabla p = \mu \nabla^2 v - \rho(\mathbf{v} \bullet \nabla)v \quad (1)$$

subject to the mass conservation constraint for incompressible flow ($\nabla \cdot \mathbf{v} = 0$), produced the velocity field v, where μ is the viscosity, p is the pressure, and ρ is the density. A zero-slip velocity boundary condition was assumed, so $\mathbf{v} = 0$ on all surfaces. A species i present in the fluid moves through a component due to convection and diffusion

$$\frac{\partial c_i}{\partial t} = -\mathbf{u} \cdot \nabla c_i + D_\mathbf{i} \nabla^2 c_i \quad (2)$$

with the concentration and diffusion coefficient denoted by c_i and D_i, respectively. Assuming the species concentration does not significantly affect the viscosity or the overall fluid density, Eq. (2) can be solved to provide the species concentration distribution after the velocity is calculated. Therefore, after the velocity field is determined, the second step solved Eq. (2) to provide the concentration distribution assuming a diffusion coefficient typical of a low molecular weight solute. The third step modeled the electric field confinement. Electric field was modeled for DC current input solving the point form of Ohm's law using the balance equation for current density given by

$$\nabla \bullet (-\sigma \nabla V) = 0 \quad (3)$$

where V is electric potential and σ is the conductivity, which in this case was based on the concentration distribution that was solved for during the second simulation step.

The baseline channel geometry for the computational modelling retained the step from a channel height of 150 μm upstream from

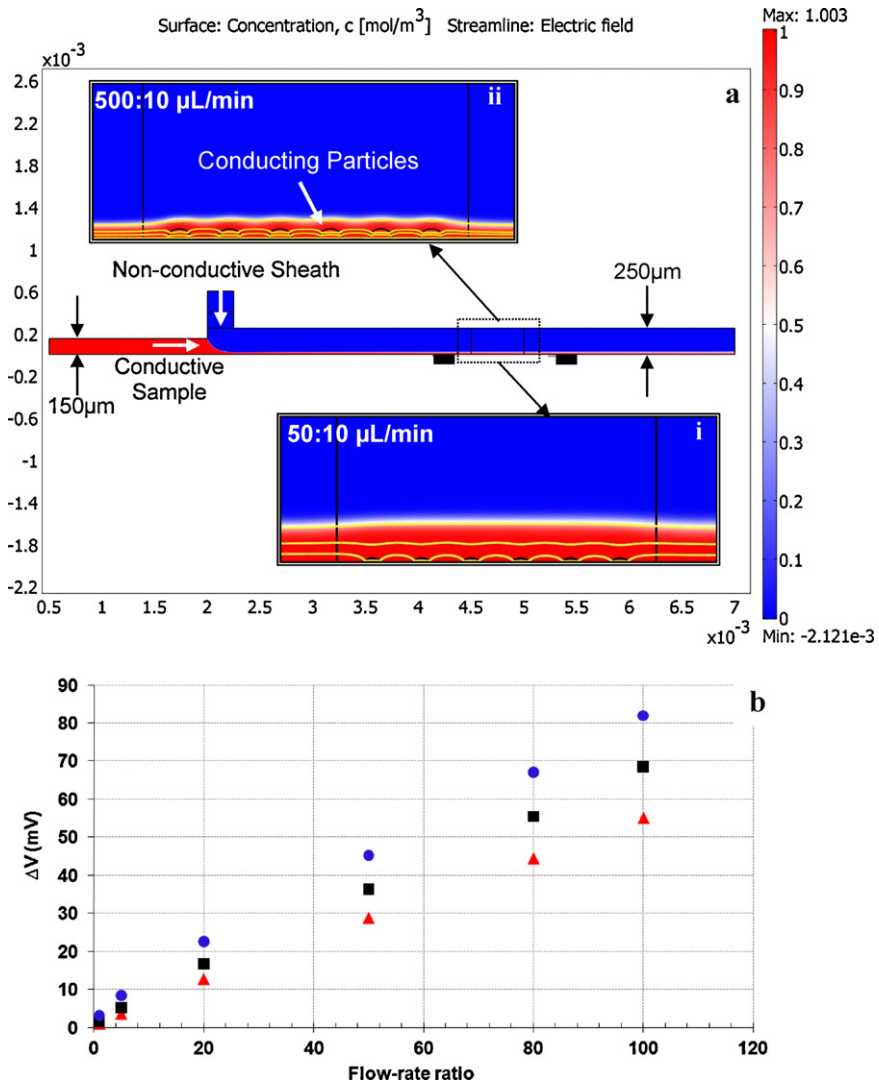

Fig. 3. (a) The results of concentration distribution using COMSOL simulation in 2D shows the conductive sample stream (in red) focused by the non-conductive sheath stream (in blue). A constant current of 1 μA is applied to one of the outer electrodes while the other is grounded. Potential difference is measured between the vertical lines. The simulations are repeated with and without the conducting particles in the sensing region. Inset (i) shows the simulation when the sheath-to-sample flow-rate ratio is 50:10 μL/min. Inset (ii) shows the case when this ratio is 500:10 μL/min. The streamlines highlight the electric field line path. (b) The results of simulations with six 15 μm × 40 μm particles (▲), six 30 μm × 40 μm particles (■) and eleven 30 μm × 40 μm particles (●). The graph has been normalized for the case when no particles are present. (For interpretation of the references to colour in this figure legend, the reader is referred to the web version of the article.)

the sheath inlet to 250 μm downstream from the sheath inlet. The sheath fluid inlet was 250 μm wide. For 3D simulations, channel symmetry was used to simulate only half the width of the actual 1 mm channel, which reduced the computation time. In order to resolve the mass transport along the interface between the sheath and sample streams accurately, adaptive meshing was used with high mesh density where needed when solving Eq. (2). The inlet flows were specified by choosing volumetric flow rates that matched the ones used in confocal studies. For mass transport simulation, a diffusion coefficient D of 1×10^{-10} m^2/s was chosen, which is a typical value for most commonly used dyes (Culbertson et al., 2002).

The conductivity of the sheath fluid was assumed to be that of deionized water ($\sigma = 5 \times 10^{-8}$ S/m) while the sample fluid was assumed to have the conductivity of phosphate buffer saline (PBS) ($\sigma = 1.5$ S/m) (Johnson et al., 2005). The particles were modeled as half-oval COMSOL sub-domains. Two different sized particles were modeled, employing a short axis length of 15 μm for smaller particles and 30 μm for larger particles. The longer axis length was 40 μm for both particle sizes. The effect of cell density was modeled by increasing the number of particles from 6 to 11 while keeping the size constant. The particles were assumed to be either insulating, e.g. cells and latex beads ($\sigma = 1 \times 10^{-9}$ S/m), or conducting, e.g. magnetic beads ($\sigma = 1 \times 10^{4}$ S/m). Two boundary elements along the bottom surface of the channel served as the electrodes (Fig. 3a). A constant DC current of 1 μA was used to calculate the current density which was applied to one electrode while the other electrode was set to ground. Potential difference was measured between two specified points for all iterations of the model. The parameters varied were the sheath and sample flow rates as well as the size, density and conductivity of the particles. The direct SPOOLES solver was used to generate the solutions.

3. Results and discussion

A model sensor was created that employs hydrodynamic focusing to confine a conducting sample stream. The slower flowing sample fluid was introduced in the first inlet and the faster flowing sheath fluid entered from the second inlet, focusing the sample

stream along the glass surface. By choosing low-conductivity deionized water for sheath flow and high-conductivity PBS solution for sample flow, the electric field generated by the passage of current through the outer two electrodes was confined to the focused sample stream. To utilize the system as a biosensor, particles or cells carried by the sample fluid should generate a change in the resistance as they are captured in the conducting fluid between the sensing electrodes. Changing the sheath-to-sample flow-rate ratio should tune the detection sensitivity of the sensor. Thus the same platform can be used for high-throughput detection of a wide range of target cells or particles without the risk of clogging. It should be noted that the T-junction design fulfils the need for the focused conductive stream to be in constant contact with the bottom surface of the channel exhibiting the microfabricated electrodes.

The degree of confinement of the conducting stream depended on the ratio of sample and sheath flow rates, as verified by the results of COMSOL simulations (Fig. 3a). If the particles were insulating, as the focused layer height becomes smaller, the electric field lines were forced to go around the particles. In the case of conductive particles, such as magnetic beads, the electric field lines curved towards the particles. When the focused layer was large, the field lines that were far away from the conducting particles were largely unaffected while the ones close to the particles were pulled towards them (Fig. 3a, inset i). As the layer was increasingly focused, the electric field density increased since the same number of field lines was packed in a smaller area. In addition, the number of field lines passing through the conducting particles increased and the potential drop between the sensing points became smaller compared to the case when particles were absent (Fig. 3a, inset ii). The simulation indicated that the change in voltage was linear with respect to the flow-rate ratio (Fig. 3b). Also simulations with larger particles resulted in greater potential drop as compared to smaller particles at same flow-focusing conditions. Likewise, with the size constant, increasing the number of cells also resulted in an increase in potential drop. The simulations verified that both the size and the density of particles affect the measured potential drop between the sensing electrodes.

As an experimental proof-of-principle, 2 μm magnetic beads (Bioclone Inc MMI-105) were trapped in the area between the two sense electrodes using a permanent magnet placed outside and just beneath the channel. The particles were passed through the channel between the sample and outlet without the focusing effect of the sheath stream. Particles can also be easily introduced in the sample stream with flow focusing. This method will be especially useful for highly efficient specific cell binding as it increases the likelihood of interaction between targets and recognition molecules (Hofmann et al., 2002). Fig. 4 shows the measured voltage with and without the beads for different flow-rate ratios. As expected, the voltage (and the resistance since the current was constant) decreased in the presence of the conductive beads. More importantly, the change became greater as the sample stream was focused more using higher flow-rate ratios. This increase in the measured signal highlighted the ability to tune the sensitivity of the conductivity sensor using flow-focusing. Comparing the trends of the simulation and experimental results with conductive particles, it can be seen that the simulation predicted an almost linear relationship between flow-rate ratios and change in voltage. However, in the actual experiments the sensitivity began to taper off as the flow-rate ratios continued to increase.

The reason for this divergence between the simulation and experiment at higher-flow rate was investigated in more detail. Confocal microscopy was used to visualize the channel cross-section at different flow-rate ratios (Fig. 5a). As the sheath flow rate increased and the sample fluid was focused towards the bottom surface of the channel, the curvature in the concentration profile increased (Fig. 5b–d). For very high flow-rate ratios, the sample fluid split into two separate streams that flowed along the bottom corners of the channel. There was also a dramatic increase in curvature of the concentration profile when both sheath and sample flow rates were increased while maintaining a flow-rate ratio of 10 (Fig. 5e–g).

As shown in the confocal images, the cusps in the focused layer increased as the Reynolds number increased. The Reynolds number *Re*, which signifies the relative importance of inertial forces versus the viscous forces in any fluid, is given by the equation:

$$Re = \frac{\rho L v}{\mu} \tag{4}$$

where ρ is the fluid density, v is the fluid velocity and μ is the dynamic fluid viscosity. L is the characteristic length which for a microchannel with rectangular cross-section is given by

$$L = \frac{4 \times \text{Area}}{\text{Perimeter}} \tag{5}$$

When the sample and sheath fluids meet at the 90° T-junction in the microfluidic channel, the velocity fields of the two streams interact and they impart the momentum they carry onto each other. The sheath fluid, which must flow faster in order to focus the sample stream, carries a greater momentum and pushes the slower flowing sample fluid towards the channel walls. Due to the parabolic

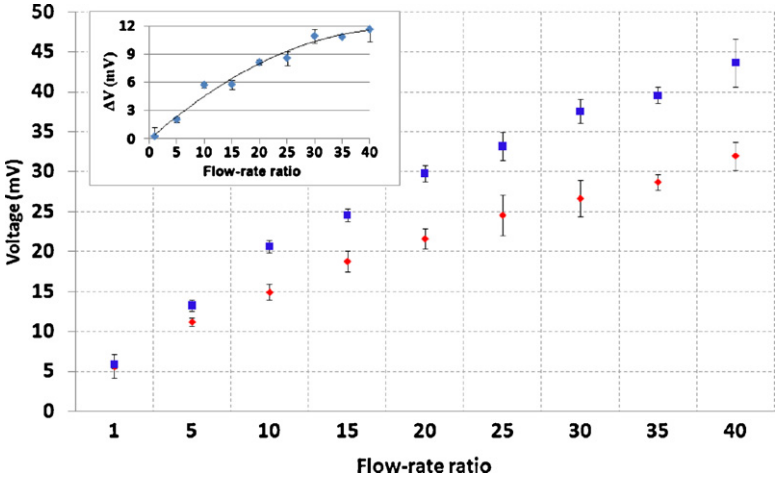

Fig. 4. The voltage between the sensing electrodes was measured for two cases: with (●) and without (■) 2 μm magnetic beads and reflects the mean ± standard deviation of three sample points. The sample flow rate was 10 μL/min for all cases. The inset shows the voltage difference between the two cases.

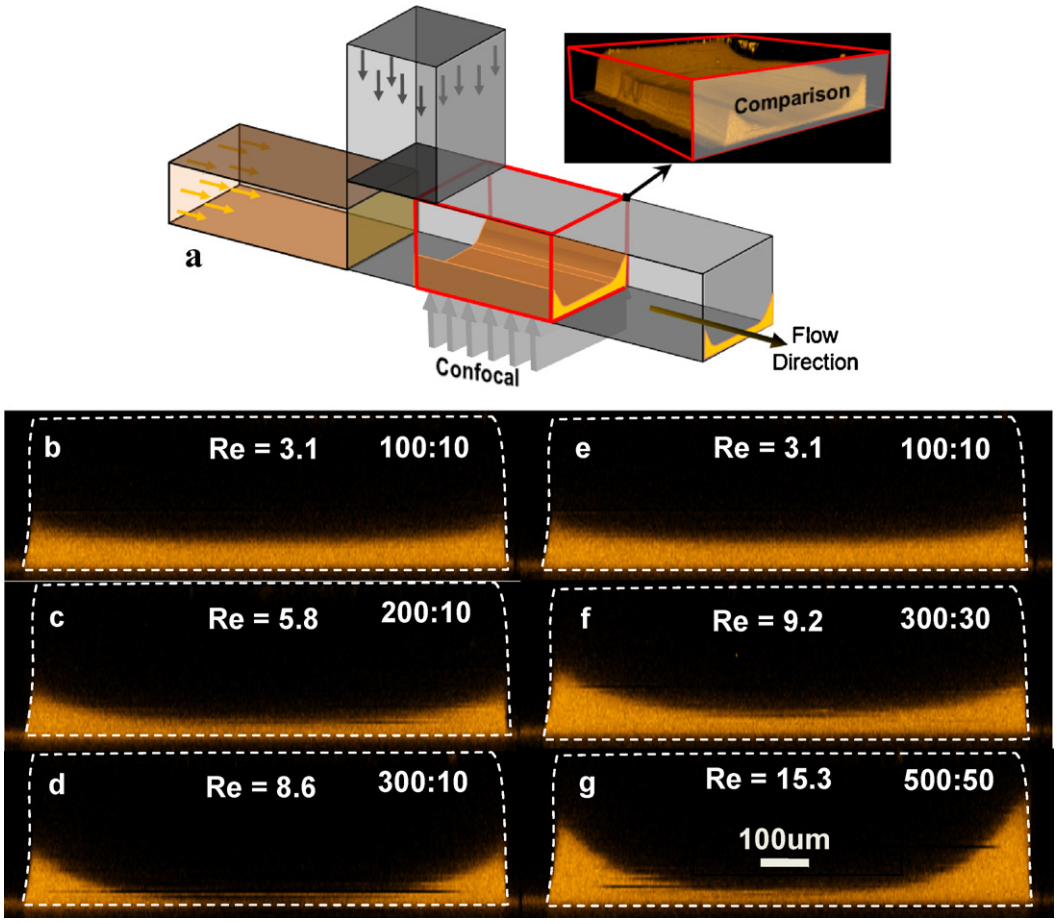

Fig. 5. (a) Diagram of the fluid focusing channel showing sheath fluid inlet (vertical), sample stream inlet (horizontal) and the section of the channel that is imaged with the confocal microscope (inset). The shaded face shown in the inset is used for comparison between different conditions of flow rates and fluid properties. 2D confocal slices (b–g) of the 3D imaged sections are compared for different sheath-to-sample ratios. (b–d) This series of confocal images shows the effects of increasing flow-rate ratio on the concentration profile of the focused stream. (e–g) This series of confocal images shows the effect of changing both flow rates while maintaining a flow-rate ratio of 10. The fluid viscosity and density were respectively 1×10^{-3} Pa s and 1×10^{3} kg/m^3 for all tests. *Re* numbers were calculated based on the channel dimensions and the flow rates.

velocity profile of the sheath flow, the sample fluid is restricted from flowing straight along the center of the channel where sheath flow velocity is highest. Since in a closed channel, the mass must be conserved, the sample fluid thus accelerates closer to the walls and decelerates at the center, which results in the formation of the cusps seen in the confocal images (see Fig. S1 in supplemental information). Since the formation of cusps is a direct result of the interaction between the parabolic velocity profiles of sheath and sample fluid, reducing the surface roughness as well as increasing the hydrophilicity of the channel walls can help achieve uniform focused streams. Several methods have been suggested to increase the hydrophilic nature of PMMA in the literature (Lim et al., 2001; Shinohara et al., 2008).

For optimum capture of cells or particles, the sample fluid needs to be focused uniformly along the bottom surface of the channel between the sense electrodes. If the target analytes are added to the sample stream for capture in real-time with flow focusing, then the formation of cusps will reduce binding or capture efficiency since many particles will pass through the cusps without coming in contact with the binding molecules on the sensing surface. As the flow rates and corresponding *Re* increased, the height of the focused stream in the middle of the channel decreased while the cusps simultaneously increased. The electric field lines passing through the cusps would thus increase with higher flow rates. In the case of magnetic beads, if the number of beads remains roughly the same, then the gain in sensitivity due to flow focusing would be countered by the loss in sensitivity due to formation of cusps, resulting in a net gain that is nonlinear with respect to flow-rate ratio (inset Fig. 4). In actual experiments, the reduction in sensitivity due to formation of cusps was compounded by the removal of the target analytes due to fluidic shear forces; this was a problem that also worsens as the flow rates continue to increase.

The discrepancy between the simulation (linear) and experiments (asymptotic) occurred because the 2D models could not accurately simulate the formation of cusps in the focused stream and the model implicitly assumed that the focused stream (Fig. 3a) extended exactly and infinitely in the third dimension. The effect of the cusps on the electric field became clearer when the results of numerical simulations were considered using a 3D geometry. At lower flow rates, the sample stream focused to a flat layer along the bottom surface of the channel. Consequently, the current density was uniform across the width of the focused stream (Fig. 6a). As the sheath flow rate increased, the focused stream height decreased near the center of the channel while cusps developed along the boundary of the channel. The non-planar shape of the focused stream implied that there are regions of varying electrical resistance across the width of the stream. As a result, the current density is no longer uniform and most of the current passes through the cusps which results in a loss of sensitivity (Fig. 6b).

If the flow rates are too high then the shear on the captured particles can also shear the particles away from between the electrodes and cause a loss in sensitivity. At the other end of spectrum, if the flow rates are too slow, then the diffusive mixing between sheath and sample fluids reduces the electric field confinement and

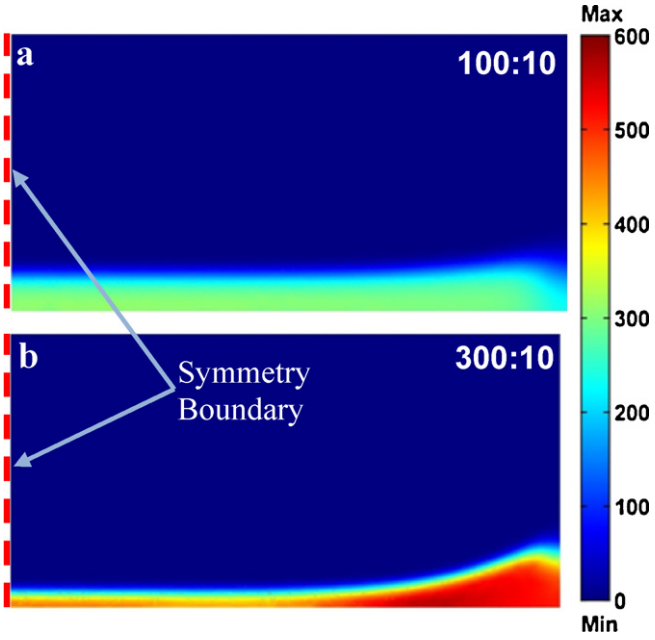

Fig. 6. Channel cross-sections show the results of finite element simulation in 3D using COMSOL for two different cases of sheath-to-sample flow-rate ratios (a) 100:10 μL/min and (b) 300:10 μL/min. Both cross-sections were been plotted on the same current density scale for comparison. Only half of the channel was simulated, assuming symmetry, to reduce computation time.

again there will be a loss of sensitivity. The results of the experiments suggested that, depending on the geometry and dimensions, there is an optimal flow-rate ratio for which the sensitivity is maximized. For the chosen dimensions of the T-junction microchannel, this optimization translated into flow rates where *Re* is less than 5.

4. Conclusion

A proof-of-principle is demonstrated for a conductance-based biosensor that uses hydrodynamic focusing to confine the conducting fluid near the surface of the sensing electrodes. Parameters critical to sensitivity include: (1) the height of the conducting stream which is defined by the relative flow rates of the focusing and conducting fluids, (2) the shape of the conducting stream as determined by the Reynolds number and geometry of the system, and (3) the conducting or insulating capacity of particles or cells immobilized between the sensing electrodes. The impact of the height and geometry of the conducting stream has been documented here. The detection of the particles between the sensing electrodes has also been proven. Further experiments are ongoing to characterize the impact of particle size and conductance on signal generation.

The shape of the hydrodynamically focused conducting stream is a factor that is not generally appreciated. In contrast to previous studies that only image a two-dimensional projection of the fluid focusing profile, this theoretical and experimental investigation of hydrodynamic focusing reveals more complex interfacial profiles at Reynolds numbers and laminar flow conditions typical for microfluidic sensors. The interaction between the velocity profiles of sample and sheath streams at the region where they first come into contact inside the microchannel play an important role in shaping the focused stream. Both modelling and microscopy indicate that although the flows are well within the laminar flow regime, the velocity profile of the faster flowing sheath fluid plays a significant role in shaping the focused stream. Reducing the Reynolds number is one approach to produce a focused fluid layer that is planar across the width of the channel.

In the sensor described here, there is clearly a point where increasing the flow-rate ratio ceases to generate a further increases in sensitivity. The modelling and conductivity evaluations indicate that at high flow-rate ratios, most of the current flows through the cusps and there is a possibility that the increasing shear forces can displace the particles. Both of these effects can offset the gains in sensitivity due to the reduced height of the conducting stream in the center of the channel. This is not the only system where inertial forces have been documented at Reynolds numbers between 1 and 90 (Di Carlo et al., 2007; Sudarsan and Ugaz, 2006a,b). Control over the shape of the focused stream is important in many biosensors and lab-on-a-chip devices, and the impact should not be underestimated.

Acknowledgements

This project is funded by the Defense Threat Reduction Agency (DTRA #AA07CBT015). The authors would like to thank Dr. David Mott at NRL for his discussions on fluid dynamics. Daniel Ateya and Mansoor Nasir are National Research Council (NRC) Postdoctoral Fellows. Diana Burk was an undergraduate summer intern with the Navy Research Enterprise Internship Program (NREIP). The views are those of the authors and do not represent the opinion or policy of the US Navy or Department of Defense.

Appendix A. Supplementary data

Supplementary data associated with this article can be found, in the online version, at doi:10.1016/j.bios.2009.10.033.

References

Atencia, J., Beebe, D.J., 2005. Nature 437, 648–655.
Brody, J.P., Yager, P., Goldstein, R.E., Austin, R.H., 1996. Biophysical Journal 71, 3430–3441.
Culbertson, C.T., Jacobson, S.C., Michael Ramsey, J., 2002. Talanta 56, 365–373.
Di Carlo, D., Irimia, D., Tompkins, R.G., Toner, M., 2007. Proceedings of the National Academy of Sciences 104, 18892.
Golden, J.P., Floyd-Smith, T.M., Mott, D.R., Ligler, F.S., 2007. Biosensors and Bioelectronics 22, 2763–2767.
Hatch, A., Kamholz, A.E., Hawkins, K.R., Munson, M.S., Schilling, E.A., Weigl, B.H., Yager, P., 2001. Nature Biotechnology 19, 461–465.
Hofmann, O., Voirin, G., Niedermann, P., Manz, A., 2002. Analytical Chemistry 74, 5243–5250.
Hua, S.Z., Pennell, T., 2009. Lab on a Chip 9, 251–256.
Huh, D., Bahng, J.H., Ling, Y., Wei, H.H., Kripfgans, O.D., Fowlkes, J.B., Grotberg, J.B., Takayama, S., 2007. Analytical Chemistry 79, 1369–1376.
Huh, D., Gu, W., Kamotani, Y., Grotberg, J.B., Takayama, S., 2005. Physiological Measurement 26, 73.
Ismagilov, R.F., Stroock, A.D., Kenis, P.J.A., Whitesides, G., Stone, H.A., 2000. Applied Physics Letters 76, 2376.
Johnson, A.M., Sadoway, D.R., Cima, M.J., Langer, R., 2005. Journal of the Electrochemical Society 152, H6.
Larsen, U.D., Blankenstein, G., Branebjerg, J., 1997. Solid State Sensors and Actuators (Transducers '97 Chicago).
Leatzow, D.M., Dodson, J.M., Golden, J.P., Ligler, F.S., 2002. Biosensors and Bioelectronics 17, 105–110.
Lee, G.B., Chang, C.C., Huang, S.B., Yang, R.J., 2006. Journal of Micromechanics and Microengineering 16, 1024–1032.
Lim, H., Lee, Y., Han, S., Cho, J., Kim, K.J., 2001. Journal of Vacuum Science & Technology A: Vacuum, Surfaces, and Films 19, 1490.
Munson, M.S., Hasenbank, M.S., Fu, E., Yager, P., 2004. Lab on a Chip 4, 438–445.
Radke, S.M., Alocilja, E.C., 2005. Biosensors and Bioelectronics 20, 1662–1667.
Rodriguez-Trujillo, R., Castillo-Fernandez, O., Garrido, M., Arundell, M., Valencia, A., Gomila, G., 2008. Biosensors and Bioelectronics 24, 290–296.
Schwan, H.P., 1968. Annals of the New York Academy of Sciences 148, 191–209.
Shinohara, H., Takahashi, Y., Mizuno, J., Shoji, S., 2008. Sensors & Actuators B: Chemical 132, 374–379.
Simonnet, C., Groisman, A., 2006. Analytical Chemistry 78, 5653–5663.
Stiles, T., Fallon, R., Vestad, T., Oakey, J., Marr, D.W.M., Squier, J., Jimenez, R., 2005. Microfluidics and Nanofluidics 1, 280–283.
Sudarsan, A.P., Ugaz, V.M., 2006a. Lab on a Chip 6, 74–82.
Sudarsan, A.P., Ugaz, V.M., 2006b. Proceedings of the National Academy of Sciences 103, 7228–7233.
Walsh, P.A., Walsh, E.J., Davies, M.R.D., 2007. International Journal of Heat and Fluid Flow 28, 44–53.